Droplet transportation by adjusting the temporal phase shift of surface acoustic waves in the Exciter-Exciter mode

Mingyang Sui,[a] Huijuan Dong,*[a] Guanyu Mu,[a] Jingze Xia,[a] Jie Zhao,*[a] Zhen Yang,*[b] Tianlong Li,[a] Tong Sun[c] and Kenneth T. V. Grattan[a,c]

[a] *State Key Laboratory of Robotics and System, Harbin Institute of Technology, Harbin, 150001, Heilongjiang Province, China.*
[b] *Institute of Orthopedics, Chinese PLA General Hospital, Beijing Key Laboratory of Regenerative Medicine in Orthopedics, Key Laboratory of Musculoskeletal Trauma & War Injuries PLA, Beijing, 100853, China.*
[c] *School of Mathematics, Computer Science and Engineering, City, University of London, London, EC1V 0HB, UK.*

Abstract: Droplet actuation using Surface Acoustic Wave (SAW) technology has been widely employed in 'lab-on-a-chip' applications, such as for on-chip Polymerase Chain Reactions. The current strategy uses the Exciter-Absorber mode (exciting a single InterDigital Transducer, IDT) to form a pure Travelling Surface Acoustic Wave (TSAW) and to actuate the droplet, where the velocity and direction of the droplet can be adjusted by controlling the on-off and amplitude of the excitation signals applied to a pair of IDTs. Herein, in a way that is different from using the Exciter-Absorber mode, we propose a method of actuating droplets by using the Exciter-Exciter mode (exciting a pair of IDTs simultaneously), where the velocity and directional adjustment of the droplet can be realized by changing only one excitation parameter for the signals (the temporal phase shift, θ), and the droplet velocity can also be significantly improved. Specifically, we report for the first time the equation of the vibration of the mixed waves (TSAW and Standing Surface Acoustic Wave (SSAW)) formed on the substrate surface using the Exciter-Exciter mode. This is analyzed theoretically, where it is shown in this work that the amplitude and direction of the TSAW component of the mixed waves can be adjusted by changing θ. Following that, the velocity and directional adjustment of the droplet has been realized by changing θ and the improvement of the droplet velocity has been verified on a one-dimensional SAW device, using this Exciter-Exciter mode. Moreover a series of experiments on droplet transportation, along different trajectories in an *x-y* plane, has been carried out using a two-dimensional SAW device and this has demonstrated the effectiveness of the θ *changing*-based approach. Here this Exciter-Exciter mode provides an alternative method for the transportation of droplets in 'lab-on-a-chip' applications.

1. Introduction

Microfluidics has been an important technology in the field of chemical analysis [1] and biomedical research [2,3] for many years, widely employed in applications such as high-throughput screening [4,5], cell and tissue separation [6], and biochemical synthesis [7]. Here droplet manipulation is an important branch of microfluidic technology. For decades, microfluidic technology has been combined with various techniques based on different physical principles such as hydrodynamics [8,9], electrodynamics [10] and electromagnetism [11,12] to manipulate droplets. In addition to these, the technology of acoustofluidics [13] can be created through a combination of acoustics and microfluidics [14-16], an approach which is important due to its property of being label-free [17] and showing high biocompatibility [18,19]. In the acoustofluidics applications reported, Bulk Acoustic Waves (BAWs) [20], acoustic streaming [21], and Surface Acoustic Waves (SAWs) [22] are usually used to manipulate the droplets. The standing BAWs can be used to actuate the levitated droplets in three-dimensional space without any contact being made [23,24]. The manipulation of droplets uses acoustic streaming technology, that is capturing and actuating droplets floating on a layer of oil which is applied to the surface of a substrate, in which hydrodynamic traps induced by the acoustic streaming can be formed in the oil. This has shown great value in applications to droplet merging and splitting [25], reagent mixing and so on [26], where the main characteristics seen are being contactless and allowing programmability [27].

In contrast, droplet manipulation using SAW technology refers to actuating the droplet using the acoustic pressure gradient formed inside the droplet, which is coupled with the SAW (where the droplet has a size much larger than the wavelength of the SAW) [28-30]. Specifically, when the droplet is placed in the propagation path of the Travelling Surface Acoustic Wave (TSAW, which can be formed on the surface of a piezoelectric substrate by exciting the InterDigital Transducers, IDTs), the acoustic energy can be radiated into the droplets to create an acoustic pressure gradient within them [31], and a sufficiently large pressure gradient will drive the droplets [32-34]. This SAW-based droplet manipulation technology shows several advantages, including small equipment size [35,36], convenience for an experimental setup and modular integration [37-39], features which have been widely employed in some 'lab-on-a-chip' applications, such as on-chip Polymerase Chain Reactions (PCR) [1,40], on-chip collection of microorganisms [41], and the transmission and merging of sample reagents [19,42,43].

The Exciter-Absorber mode (termed here the E-A mode) [44-46], has been routinely used to drive droplets in existing SAW-based droplet actuation applications. Specifically, a radio frequency signal is applied to a single IDT to generate a pure TSAW, which then propagates on the surface of the piezoelectric substrate, and thus the droplet on the substrate can be actuated to move along the same direction as the TSAW [47,48]. When driving droplets in a straight line using the E-A mode, it is necessary to control the on-off and amplitude of the excitation signals of two IDTs respectively, in order to adjust the velocity and direction of the actuated droplet.

Herein, in a way that is different from using the E-A mode, a method of actuating droplets by using the Exciter-Exciter mode has been proposed by the authors (*i.e.*, exciting a pair of opposite IDTs at the same time, termed here the E-E mode).

Two advantages of the use of this E-E mode in actuating droplets have been theoretically analyzed and experimentally proved: (1) the velocity and direction of the actuated droplet could be adjusted by changing only one excitation parameter for the signals (temporal phase shift, θ), and (2) the velocity of the actuated droplet could be significantly increased. Here this E-E mode has the potential to be a useful alternative to the traditional E-A mode for the actuation of the droplets, and it will benefit some 'lab-on-a-chip' applications using the SAW-based droplet manipulation technology, where not only can the control of the reagent transmission be simplified, but also its velocity can be improved.

In this paper, considering the reflection of the surface acoustic wave at the IDTs in the open SAW device used in the E-E mode (which was usually ignored in previous studies), we report for the first time the equation for the mechanical vibration of the mixed waves (TSAWs and Standing Surface Acoustic Waves, SSAWs), formed on the substrate surface by using the E-E mode. Following that, the amplitude and direction of the TSAW component in the mixed waves have been theoretically analyzed, where these can be adjusted by changing the frequency or the phase shift of the excitation signals applied to the two IDTs. Thus, the adjustment of the velocity and direction of the droplet can be realized. Here an experiment to investigate the adjustment of the velocity and direction has been carried out using a one-dimensional SAW device, where the effectiveness of the θ changing-based approach and the associated improvement in the droplet velocity have been demonstrated. In addition, a two-dimensional SAW device with two pairs of orthogonal IDTs has been developed, where the temporal phase shifts in the E-E mode were used to control the droplets moving along different complex routes in an *x-y* plane. It is noted here that the E-E mode is used to actuate droplets of a size much larger than the wavelength of the surface acoustic wave. However, in previous studies, the E-E mode was often used to generate a pure SSAW in the microchannel placed on the substrate of a SAW device, where frequency or phase control of the IDTs had been employed to change the positions of the standing wave nodes and thus the particles or cells captured by the nodes could be manipulated [49-51]. However, these situations are different from the major objective and the key driving principle of the research reported herein.

2. Underpinning theoretical background

2.1. Description of the amplitude of the TSAWs

A schematic of the vibration of the mixed TSAWs and SSAWs on the surface of a piezoelectric substrate in the E-E mode can be seen in Fig. 1. The surface acoustic waves (SAWs) generated by each pair of fingers in the IDT are superimposed on each other, considering here the incident SAW being generated along the center line of each IDT. Taking IDT $1^{\#}$ as an example, when the incident wave generated by IDT $1^{\#}$ propagates along the substrate surface to IDT $2^{\#}$ on the opposite side, electric reflection based on the acoustoelectric reemission, and acoustic reflection based on the different acoustic impedances between the transducer and the substrate is caused. It is assumed here that the incident SAW excited by IDT $1^{\#}$ will be totally reflected from the center line of IDT $2^{\#}$, where *L* represents the distance between the incident center and the reflection center. It is assumed that the incident and reflected waves generated by IDT $2^{\#}$ are created in a similar way. Here θ represents the temporal phase shift of the two signals applied to the two IDTs.
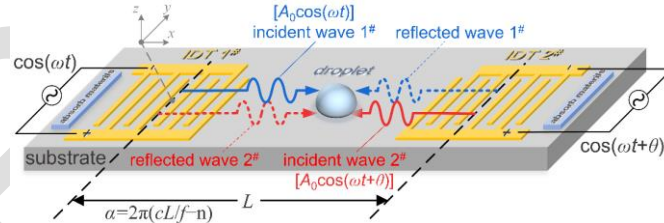

Fig. 1 Schematic of the excitation principle of the mixture of TSAWs and SSAWs using the SAW device in the Exciter-Exciter mode. The red and blue solid lines represent the incident wave, $A_0\cdot\cos(\omega t)$ and $A_0\cdot\cos(\omega t+\theta)$, excited by IDT $1^{\#}$ and IDT $2^{\#}$ respectively, and the red and blue dotted lines represent the corresponding reflected waves respectively (A_0 represents the amplitude of the incident wave, that is a TSAW generated by one IDT).

As shown in Fig. 1, IDT $1^{\#}$ and IDT $2^{\#}$ respectively generate TSAWs which will be totally reflected from the opposing side, and the incident wave and the reflected wave are superimposed to form SSAW $1^{\#}$ and SSAW $2^{\#}$, where here the two SSAWs are superimposed symmetrically, without considering the effects of half-wave loss and the influence of the plate length on the reflection. Following that, the vibrational displacement along the *z* direction of each particle on the substrate surface at time, *t*, and at a position, *x*, can be written as [52,53]:

$$d_z(x,t) = 2A_0[\cos\omega t\cos kx + \cos(\omega t + \theta)\cos(kx + kL)]$$

Here the *spatial phase difference*, $\alpha = kL - n\cdot 2\pi = 2\pi\cdot(\frac{cL}{f}-n)$, where *k* represents the wavenumber of the SAW, *c* and *f* respectively represent the speed of the SAW propagating on the substrate and the excitation frequency of the signals, where $\omega = 2\pi f$, and *n* is an integer where $\alpha \in [0, 2\pi)$, and thus the above equation can be rewritten as:

$$d_z(x,t) = 2A_0[\cos\omega t\cos kx + \cos(\omega t + \theta)\cos(kx + \alpha)] \tag{1}$$

Here, as seen in Eq. 1, the two standing waves are numerically simulated and superimposed on each other. Pure SSAWs, pure TSAWs or mixed waves of the two on the substrate can be formed when adjusting θ or α, and the corresponding curves representing the *x* positions and vibrational displacement (*z*-axis) are shown in Fig. 2. As can be seen from the illustrations in the figure, A_{max} (shown by the dashed lines) and A_{min} (shown by the dash-dotted lines), represent the amplitudes of the SSAWs (A_{SSAW}) and the amplitudes of the TSAWs (A_{TSAW}), respectively [54,55]. The pure TSAWs can be formed when A_{max} equals A_{min}, where A_{TSAW} reaches its maximum value, $A_{pure\ TSAW}$.
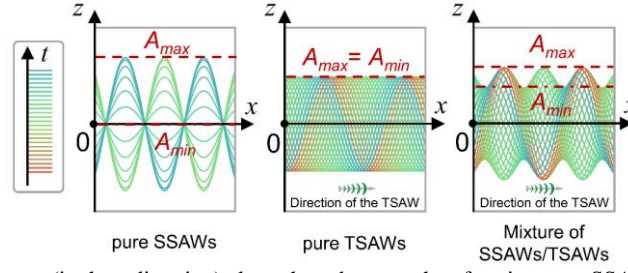
Fig. 2 Graphs of the vibrational displacement (in the *z* direction) along the substrate when forming *pure* SSAWs, *pure* TSAWs or a mixture of SSAWs and TSAWs on the substrate. Here different coloured curves are used to represent the vibrational displacements at different times. The dashed lines show the maximum amplitudes (A_{max}) of all the particles on the surface of the substrate, and the dash-dotted line shows the minimum amplitudes (A_{min}), that is, the amplitude of the TSAW component, A_{TSAW}.

2.2. Methods for the amplitude and directional adjustment of the TSAWs by changing θ or α

Method for adjustment of the amplitudes of the TSAWs. Here the amplitudes of the TSAW component, A_{TSAW}, propagating along the *x*-axis on the substrate, can be derived from Eq. 1 and is given by Eq. 2. (It should be noted that the TSAWs in the E-E mode mentioned later in this paper refers to the TSAW component of the mixed waves).

$$A_{TSAW} = A_{min} = \min\left(2A_0 \left|2\sin\frac{\alpha}{2}\sin\frac{\theta}{2}\right|, 2A_0\left|2\cos\frac{\alpha}{2}\cos\frac{\theta}{2}\right|\right) = \begin{cases} 2A_0\left|2\sin\frac{\alpha}{2}\sin\frac{\theta}{2}\right| & (0 < \theta < \theta_1, \theta_2 < \theta < 2\pi) \\ 2A_0\left|2\cos\frac{\alpha}{2}\cos\frac{\theta}{2}\right| & (\theta_1 \le \theta \le \theta_2) \end{cases} \quad (2)$$

where θ_1 and θ_2 are the two special values of θ which occur when $\left|2\sin\frac{\alpha}{2}\sin\frac{\theta}{2}\right| = \left|2\cos\frac{\alpha}{2}\cos\frac{\theta}{2}\right|$, and in this case, the value of A_{TSAW} reached a maximum, $A_{pure\ TSAW}$, that is, when the pure TSAW is formed. It can be noted that the values of θ_1 and θ_2 are related to α, and these are given by:

$$\theta_1 = \begin{cases} \pi - \alpha & (0 \le \alpha \le \pi, x+\ propagating) \\ \alpha - \pi & (\pi < \alpha \le 2\pi, x-\ propagating) \end{cases}$$
$$\theta_2 = \begin{cases} \pi + \alpha & (0 \le \alpha \le \pi, x-\ propagating) \\ 3\pi - \alpha & (\pi < \alpha \le 2\pi, x+\ propagating) \end{cases} \quad (3)$$

It is noted that the value of A_{TSAW} determines the velocity of the actuated droplet. A_{TSAW} reached its maxima when θ is set to θ_1 or θ_2, where the droplet will have its *maximum* velocity.

Accordingly, the theoretical relationship between θ, α and A_{TSAW} is shown in Fig. 3, and the relationship of the three variables is given in Fig. 3(a). Taking certain values of θ and α, the curves showing the relationship between α and A_{TSAW} (in the cases of $\theta=\pi/2$ and $\theta'=\pi/4$) are shown in Fig. 3(b), and the curves showing the relationship between θ and A_{TSAW} (in the cases of $\alpha=3\pi/2$ and $\alpha'=7\pi/4$) are shown in Fig. 3(c). By analyzing Eq. 2, in Figs. 3 (b) and (c) it can be seen that θ and α have the same effects on A_{TSAW} in the mixed waves. Here the change of θ has been taken as an example in this section, and the method to adjust the amplitude and direction of the TSAWs has been analyzed. It can be seen from Fig. 3(c) that as θ varies from 0 to 2π, there are not only two specific values of θ, θ_1 and θ_2, at which the pure TSAWs can be formed, and another two specific values of θ, 0 and π, at which the pure SSAWs can be formed, but also the two varying ranges of θ which are symmetric about π, and A_{TSAW} can be adjusted by changing θ across either range.
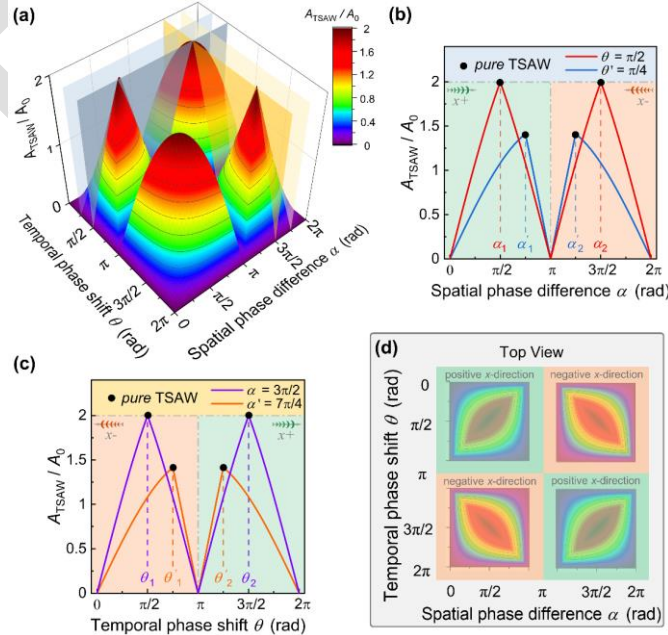
Fig. 3 Theoretical relationship relating to θ, α and A_{TSAW}. (a) Relationship of the three variables. (b) Graphs of the relationship between α and A_{TSAW} where $\theta=\pi/2$ (red curve) and $\theta=\pi/4$ (blue curve) respectively. (c) Graphs of the relationship between θ and A_{TSAW} where $\alpha=3\pi/2$ (purple curve) and $\alpha=7\pi/4$ (orange curve) respectively. The black dots in (b) and (c) indicate that pure TSAWs can be formed in this case. (d) Top view of (a), illustrating the relationship across θ, α and the direction of the TSAW components in the mixed waves, where here the green / orange areas represent the TSAWs propagating in the positive / negative x-directions respectively.

Relative maximum value of the amplitudes of the TSAWs. As can be seen from Eq. 2, for a given value of α, the pure TSAWs can be formed when θ was set to θ_1 or θ_2, in this case, the relative maximum value of the amplitude of the TSAWs, $A_{pure\,\text{TSAW}}$, can be obtained and is shown below:

$$A_{pure\,\text{TSAW}} = 2A_0 \left| \sin \alpha \right| \tag{4}$$

As shown in Eq. 4, the amplitudes of the pure TSAWs, $A_{pure\,\text{TSAW}}$, vary with the values of α. These values change in the expression, $|2A_0 \cdot \sin\alpha|$, and the relative maximum value of $A_{pure\,\text{TSAW}}$ can reach $2A_0$. As seen in Fig. 3(c), $A_{pure\,\text{TSAW}}$ reaches its relative maximum when θ_1 is adjusted to $\pi/2$ or θ_2 is equal to $3\pi/2$, in the case of α being $3\pi/2$. It is noted that the amplitude of the TSAW formed is assumed to be A_0 when exciting one IDT in the E-A mode – this means that the maximum amplitudes of the TSAWs formed can reach $2A_0$, when exciting a pair of IDTs in the E-E mode. As a result, the upper limit of the amplitudes of the TSAWs can be doubled, and thus the velocity of the actuated droplets can be significantly increased.

Method for adjustment of the directions of the TSAWs. The velocity of the actuated droplet can be described by A_{TSAW}, while its direction can be indicated by the directions of propagation of the TSAWs. The pure TSAWs can be formed on the substrate when θ is given by θ_1 or θ_2, for different ranges of α, where the vibrational displacements can be written as:

$$d_{pure\text{TSAW}}(x,t)=\begin{cases} 2A_0\sin\alpha \cdot \sin(kx-\omega t+\alpha) & (\theta=\theta_1, \alpha\in(0,\pi), x+\,propagating) \\ 2A_0\sin\alpha \cdot \sin(kx+\omega t+\alpha) & (\theta=\theta_2, \alpha\in(0,\pi), x-\,propagating) \\ 2A_0\sin\alpha \cdot \sin(kx+\omega t+\alpha) & (\theta=\theta_1, \alpha\in(\pi,2\pi), x-\,propagating) \\ 2A_0\sin\alpha \cdot \sin(kx-\omega t+\alpha) & (\theta=\theta_2, \alpha\in(\pi,2\pi), x+\,propagating) \end{cases} \tag{5}$$

As shown in Eq. 5 and Fig. 3(c), the pure TSAWs can propagate in two opposite directions when changing θ over the two ranges, $(0, \pi)$ and $(\pi, 2\pi)$, at a given value of α. Since θ and α have the same effects on the TSAWs, similarly it can be seen that the directions of the TSAWs can be also adjusted when changing α over the two ranges of $(0, \pi)$ and $(\pi, 2\pi)$, at a given value of θ. As illustrated in Fig. 3(d), here the areas shown in green represent the TSAWs (formed on the substrate) which propagate along the positive direction of the x-axis when θ and α are set within the corresponding ranges, while the areas in orange represent the TSAWs propagating in the negative x-direction.

In summary, when the mixture of the TSAWs and SSAWs is formed by using the E-E mode, both the amplitude and direction of the TSAWs can be adjusted by changing either the temporal phase shift, θ, or the spatial phase difference, α. In addition, when θ or α lies in the range of $(0, \pi)$ or $(\pi, 2\pi)$, not only are the directions of the TSAWs opposite, but also the amplitudes of the TSAWs can be continuously adjusted.

2.3. Velocity and directional adjustment of the actuated droplets by changing θ or f

When placing a droplet upon the surface of the substrate to interact with the TSAW propagating along the x-direction, generated by a single IDT, acoustic streaming will occur in the droplet of a size much greater than the acoustic wavelength in the fluid [32]. The total driving force, F_s applied to the droplet, is proportional to square of the amplitude of the TSAW [22]. Here the z direction-based displacement component of the TSAW was diffracted into the droplet at the Rayleigh angle, and the leaky component of the TSAW induces an acoustic pressure gradient inside the droplet. A numerical simulation of this was carried out, as illustrated in Fig. 4(a), where the direction of the pressure follows the Rayleigh angle, Θ_R, which is defined as $\Theta_R= \sin^{-1}(v_l/v_s)$, where v_l is the Rayleigh wave velocity in the liquid and v_s is that in the solid [41].

When the amplitude of the TSAW increases so that $F_s \cdot \sin\Theta_R$ increases beyond the pinning force of the droplet, F_{cl} (the driving force of the TSAW will lead to the asymmetric deformation of the droplet, resulting in the pinning force, F_{cl}, due to the contact angle hysteresis [56,57]), the droplet will be actuated to move along the x-axis. Previous studies have shown that the larger the amplitude of TSAW, the faster the droplet will move [47,58,59]. However, there is no lateral propagating wave component interacting with the droplet on the substrate when the pure SSAW is formed, illustrated by the simulation results shown in Fig. 4(b), and there is no total x-direction acoustic driving force. In summary, therefore, when actuating droplets using SAW technology, only TSAWs can drive the droplets, while SSAWs cannot [32,45].
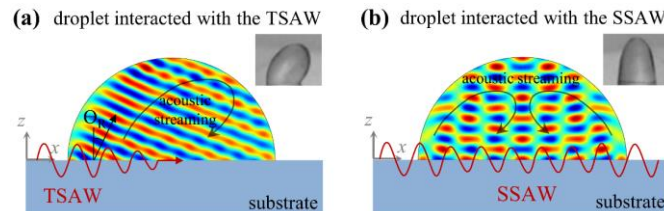

(a) droplet interacted with the TSAW   **(b)** droplet interacted with the SSAW

Fig. 4 Numerical prediction of the acoustic pressure distribution in the droplet which has interacted with (a) the TSAW and (b) the SSAW (using COMSOL Multiphysics 5.5, http://www.comsol.com). The deformations of the droplets are not shown in the simulation diagram, but the actual deformations are shown in the photograph on the right-hand side of each figure, (a) and (b).

Therefore, as discussed above, the amplitudes and directions of the TSAWs generated can be adjusted by changing θ or α when using a SAW device excited in the E-E mode. As a result, the velocities and directions of the droplets being moved on the substrate can be also controlled by the use of θ or α.

It can be noted that from the definition of α in Eq. 1 (that is, $\alpha=kL-nkc/f$), the relative distance between the two IDTs, L, and the speed of the SAW propagating on the substrate, c, are constant for a particular SAW device. α can be adjusted by changing the frequency, f, of the excitation signals, due to the fact that a SAW device can be in resonance within a particular frequency range. As a result, for an actual SAW device, the amplitude and direction of the TSAWs, in the mixed waves formed on the substrate in the E-E mode, can be adjusted by changing θ or f. This allows the velocity and direction of the actuated droplets on the substrate to be changed, as will be demonstrated in the experiments reported in the following section.

3. Experimental investigation of the velocity and direction of the droplets

3.1. One-dimensional SAW device fabrication

In this work, to verify the effectiveness of the two proposed methods for the adjustment of the velocity and direction of the droplets, a pair of IDTs was deposited in parallel on a 128° YX lithium niobate (LiNbO$_3$) piezoelectric wafer (500 μm thick) by e-beam evaporation of Cr (5 nm, adhesive layer) and Au (80 nm). The one-dimensional SAW device developed is shown in Fig. 5(a), where each IDT was composed of 30 pairs of periodically arranged finger electrodes. The interdigital period of each IDT was 100 μm and each electrode was 9 mm long and 25 μm wide, corresponding to the IDTs design frequency of 39.70 MHz. Prior to the experiment being carried out, a layer of fluorosilicone polymer was coated on the surface of the LiNbO$_3$ substrate to improve the hydrophobic and oleophobic performance, to increase the velocity of the droplets that were actuated and keep them in shape as they moved. In addition, the SAW device was mounted on an IDT-driver board, which had two signal input ports.

Here the properties of the SAW bandpass filters were used to detect the resonant frequencies of the IDTs. Specifically, a voltage of 20V, at a frequency chosen over the range from 39.0 MHz to 40.2 MHz, was applied to IDT 1$^{\#}$, while the voltages on IDT 2$^{\#}$, being used as the receiver, could be sampled and these shown in Fig. 5(b) (as the blue curve). Similarly, the voltages on IDT 1$^{\#}$, when used as the receiver, are shown in Fig. 5(b) (as the red curve). As can be seen from Fig. 5(b), the signals received from the two IDTs are highly consistent with each other. However, their resonant frequencies had shifted slightly from the theoretical design frequencies, due to both the errors during the fabrication process and the loading from the metal electrodes. The *actual* resonant frequency bandwidth of the SAW device developed was experimentally obtained to be in the range from 39.50 MHz to 39.70 MHz, and thus the excitation frequencies of the IDTs used were changed to be within this range in the experiments carried out. In addition, α was also changed over this range to adjust the velocity and direction of the droplets considered.
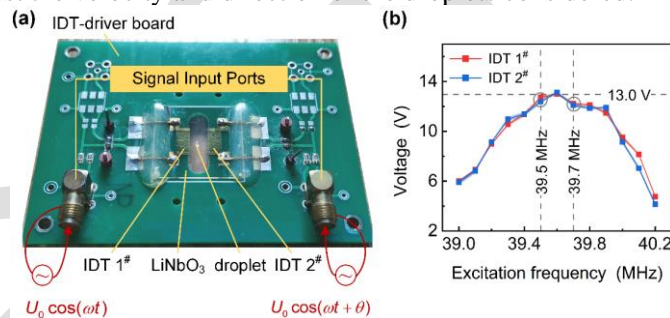

Fig. 5 SAW device developed in this work and results reported on the detection of its resonant frequency. (a) photograph of the SAW device and the IDT-driver board. (b) relationship between the values of the excitation frequency within the resonant frequency bandwidth and the voltages on the IDT being used as the receiver.

3.2. Velocity and direction adjustment of the actuated droplets, by changing θ or α

θ changing-based approach. It can be seen from the above that the velocity and direction of the actuated droplets can be adjusted by changing the value of θ. In order to demonstrate that, the developed SAW device has been used to actuate the droplets. Two sinusoidal radio frequency signals (provided by a SAW generator developed by the authors) were respectively applied to the two IDTs in parallel, these signals having the same amplitude, U_0, of 28 V, the same frequency, f, of 39.50 MHz, as well as a temporal phase shift, θ, varying from 0° to 360°. Since the propagation of the TSAWs between the two IDTs can be regarded as a flow of mechanical energy, an indirect A_{TSAW} measurement method has been used (with an oscilloscope). This was based on the energy flow approach being used to obtain the amplitudes of the voltages on these two IDTs. Specifically, the relative values of the amplitudes of the TSAWs can be represented by the absolute value of the voltage difference measured between the two IDTs, where the directions of the TSAWs are indicated by the signal direction.

In this way, the amplitude and direction of the TSAWs, varying with θ, were obtained experimentally, as shown by the red squares in Fig. 6. It can be noted that the amplitude values of the TSAWs, A_{TSAW}, calculated and measured in this work are the *relative values* (this will no longer be emphasized below). The amplitudes of the TSAWs, A_0, generated by exciting one single IDT, were used as the relative reference in the theoretical calculation, while the input voltage, U_0, applied to each IDT, can be regarded as the relative reference in the experimental measurement.
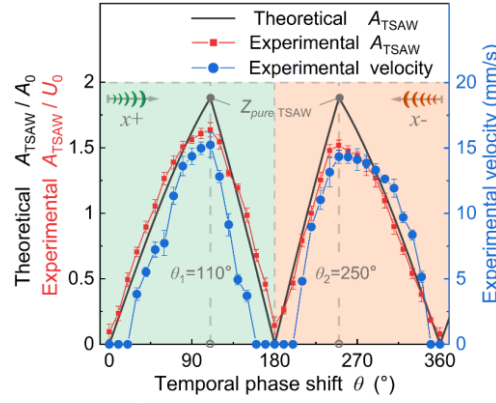
Fig. 6 A_{TSAW} and the velocities of the droplets plotted against θ. The red squares and the black curves represent the experimental values of A_{TSAW} and the theoretical relationship respectively, while the blue dots represent the average velocities, where each average value was obtained over four measurements. Here the area and the arrow (shown in green) respectively represent the TSAWs and the droplets both propagating along the positive x-direction, and *verse versa* for the area and the arrow (shown in orange) propagating in the negative x-direction. U_0=28 V, f=39.50 MHz.

Prior to these experiments being carried out, ethanol droplets were loaded onto the LiNbO$_3$ substrate using a micropipette, allowing each droplet to have a volume of about 0.8 µL and a diameter ranging from 900 to 1200 µm. The steps in the operation carried out and the environment of each test have been kept the same to avoid any interference from differences in the contact angles of the droplets, the temperature or the hydrophobicity of the substrate surface on the velocities of the droplets. Compared with the water droplets, it was easier not only to move the ethanol droplets, but also to adjust them over a wider velocity range. A high-speed video camera (type GS3-U3-51S5C-C, FLIR) was used to record the movements of the droplets at 60 frames per second, where the reading error of the center of the droplet was approximately ±1 pixel (±21 µm). As a result, the absolute error in the velocity of the droplet was approximately ±1.26 mm/s. Then the values of the velocity of the droplets, varying with θ, were obtained by processing the images of the recorded videos, and the results were plotted as the blue dots in Fig. 6. It can be seen that the droplet moved in the opposite direction when θ was changed over the two ranges, (0°<θ<180°) and (180°<θ<360°). Here, when θ was set to be 110° or 250°, not only had the values of A_{TSAW} their maxima, but also the actuated droplets reached their maximum velocities in their own directions (15.2mm/s and 14.3mm/s, respectively), and also the entire curve was symmetric about 180°. In summary, the experiments carried out have demonstrated that the directions and the velocities for the droplet can be adjusted by program-based changing of θ only, when the value of α is fixed (which means the excitation frequency, f, remains constant).

α changing-based approach. The above experiments carried out have demonstrated the effectiveness of the method to adjust the velocity and the direction of the droplets actuated, by changing the value of θ. As discussed theoretically in Section 2 (α had the same effect as θ on the TSAWs in the E-E mode), it can be concluded that the velocity and direction can also be adjusted by changing α. As discussed above, the value of α of a SAW device can be adjusted by changing the frequency, f, of the excitation signals applied to it. Here the method used for the measurement of α of the SAW device, at a series of different values of f, is described: the graph of the experimental relationship as A_{TSAW} varies with θ at a given value of f was measured, and as a result the values of θ_1 and θ_2, which correspond to the maxima of A_{TSAW} can be found. As a result, the values of α can be obtained using Eq. 3, as well as the directions of the TSAWs. Taking Fig. 6 as an example, it can be seen that A_{TSAW} reached a relative maximum at θ_1=110°, where the TSAWs propagated in the positive x-direction, and thus it can be determined that α=70° (i.e. (180°- α) = 110°). Alternatively, A_{TSAW} reached a relative maximum value at θ_2=250°, while the TSAWs propagated in the negative x-direction, and thus α can be calculated also to be 70° (i.e. (180°+ α) = 250°). Following this method of measuring α, as f increased from 39.30 MHz to 39.90 MHz (in intervals of 0.01 MHz), the values of θ_1 and the directions of the corresponding TSAWs were measured. Here the area and the arrows shown in green or orange represent the TSAWs propagating along the positive or negative x-directions, respectively: then accordingly the values of α were calculated and are shown as the red squares in Fig. 7.
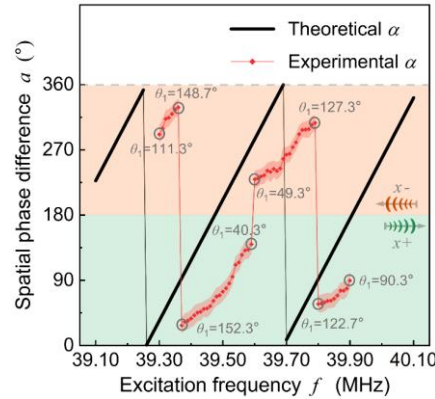

Fig. 7 Experimental and theoretical relationships between f and α. The red squares and the black graph represent the experimental values and the theoretical relationship with α, respectively.

It can be noted that the speed, c, of the SAW propagating on the 128° YX LiNbO$_3$ substrate is 3900 m/s, and the distance between the two IDTs, L, is 9.04 mm (as illustrated in Section 3.1). As a result, the relationship between f and α can be calculated theoretically, and this has been plotted as a graph (shown in black in Fig. 7), over the range of f varying from 39.10 MHz to 40.10 MHz. As can be seen from Fig. 7, the experimental values of α are highly consistent with the theoretical graph: however, part of the experimental values of α over the range of $[0,2\pi)$ cannot be obtained by changing f – in other words, there will be 'blind spots' when using the α *changing*-based approach. In addition, the amplitudes of the SAWs at a series of values of f within the resonant frequency bandwidth are different (as seen in Fig. 5(b)), which results in an interference factor during the process of the adjustment of α, by changing f. It can be concluded that of the two methods considered for the adjustment of the velocity and direction (θ *changing*-based and α *changing*-based approaches), the θ *changing*-based approach offers greater linearity and more convenience when actuating a droplet using a SAW device in the E-E mode.

3.3. *Measurement of the velocity of the droplet*

Measurement of the relative maximum velocity of the droplet. As discussed theoretically in Section 2.2, $A_{pure\ \mathrm{TSAW}}$ is equal to $|2A_0 \cdot \sin\alpha|$ at a given value of α in the E-E mode. This means that the values of $A_{pure\ \mathrm{TSAW}}$ are related to those of α (that is, related to f). In other words, there exists an optimal excitation frequency, f, at which the relative maximum velocity of the droplet can be reached.

In this work, a series of values of $A_{pure\ \mathrm{TSAW}}$ of the SAW device was experimentally measured and plotted (as shown by red squares in Fig. 8) when θ was adjusted to θ_1, for different values of f. Following that, the relative maxima of the velocities of the droplets were measured (and are shown by the blue dots in Fig. 8). Since θ_1 and θ_2 are symmetric about π, therefore, only the values of $A_{pure\ \mathrm{TSAW}}$ at θ_1 were measured in this experiment. It can be seen that the values of both $A_{pure\ \mathrm{TSAW}}$ and the relative maximum velocities reach their peaks at a frequency of 39.50 MHz.
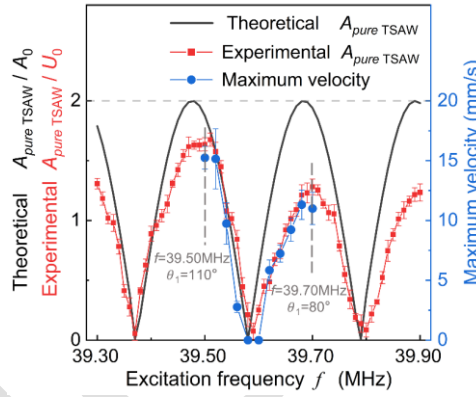

Fig. 8 Experimental and theoretical values of $A_{pure\ \mathrm{TSAW}}$ plotted against f, and the relative maximum values of the velocity of the droplet at different values of f. The input voltage, U_0=28 V, and f increased from 39.30 MHz to 39.90 MHz (in an interval of 0.01 MHz).

Velocity advantage of the actuated droplets in the E-E mode. Compared with the traditional E-A mode, the amplitudes of the pure TSAWs excited using the E-E mode, will be doubled at the same value of U_0 (as shown in Eq. 4). As a result, the droplets actuated using the E-E mode can move faster. In order to compare the velocities of the droplets actuated in the two modes, a series of experiments has been carried out using the one-dimensional SAW device developed, and the relationships between the velocities and U_0 were measured, and these are shown in Fig. 9. It can be noted that the velocity measured in the E-E mode was the maximum, which can be achieved at a given value of U_0.
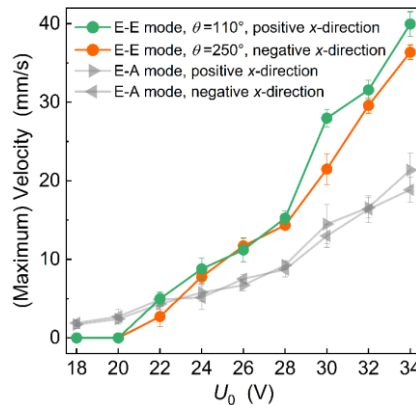

Fig. 9 Relationships between the velocities and the input voltage, U_0, in the E-A mode and the E-E mode. The gray triangles represent the velocities of the droplets driven in the E-A mode and the dots represent the maximum velocities of the droplets driven in the E-E mode. Here f=39.50 MHz, U_0 varies from 18 V to 34 V (in intervals of 2 V). The volume of droplets of each test has been kept at 0.8 μL and the steps in the operation and the environment of each test have been kept the same. It is noted that when using the E-A mode, a single IDT was activated and a layer of removable sound-absorbing adhesive was applied to cover the opposite IDT, where the sound waves propagated from the activated IDT could be temporarily absorbed and a pure TSAW without a standing wave component could be formed in the E-A mode.

As shown in Fig. 9, the droplets cannot be moved at smaller values of U_0 because there were more SSAWs remaining in the mixed waves formed on the substrate, and this prevents the droplets from being driven. As the value of U_0 was

raised, the maximum velocities of the droplets driven in the E-E mode gradually increased compared to those seen using the E-A mode. Here the velocities of the droplets driven in the E-E mode reached 39.97 mm/s in the positive x-direction and 36.38 mm/s in the negative x-direction (at U_0 equal to 34V), compared to values of only 21.38 mm/s and 18.87 mm/s respectively in the E-A mode. It can be concluded, that compared to the E-A mode, the upper limits of the velocities of the droplets can be raised using the E-E mode, as indicated, by 87.0% in the positive x-direction and 92.8% in the negative x-direction for this SAW device.

4. Transportation of a droplet in an *x-y* plane by adjusting θ

4.1. Two-dimensional SAW device fabrication

In this work, a single droplet with a volume of about 1.4 μL on the substrate has been transported by adjusting θ in the E-E mode, where a two-dimensional SAW device deposited with two pairs of orthogonal IDTs was used. The two-dimensional SAW device and its IDT-driver board developed are shown in Fig. 10 (a), where each of the four IDTs was made up of 20 pairs of electrodes deposited in parallel and spaced uniformly, with an acoustic aperture of 10 mm and an interdigital period of 300 μm. Accordingly, the design frequency of the IDTs was calculated to be 19.85 MHz, while the actual excitation frequency was measured to be 20.40 MHz. The experiments carried out have demonstrated that not only can the pure TSAWs be formed in the negative or positive directions at θ_1=80° or θ_2=280° respectively, but also the droplets can be actuated to the highest velocities.
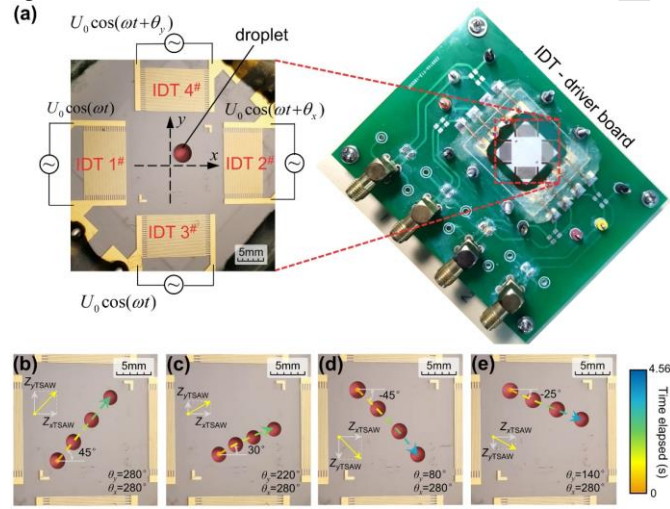

Fig. 10 Two-dimensional SAW device and the time-lapsed trajectories of the droplet transported along the oblique lines shown. (a) photograph of the SAW device with two pairs of orthogonal-placed IDTs, and the IDT-driver board. The area set for the droplet transportation was marked by the red dotted lines (and enlarged with a scale bar of 5 mm). (b)~(e) (see Video S1~S4) Time-lapsed trajectories of the droplet transported along oblique straight lines: where (b) 45°, (c) 30°, (d) -45°, and (e) -25°. Each image is a composite of four images taken at different time steps, and the central circles of the droplets were used to represent their positions (instead of the complete contours of the droplets). Here U_0=38 V, f=20.40 MHz, (Scale bars: 5mm).

4.2. Transportation of the droplet by adjusting θ in the E-E mode

The two-dimensional SAW device was used to move a droplet on the surface of the LiNbO$_3$ substrate. Here signals with an excitation frequency, f, of 20.40 MHz, and with an input voltage, U_0, of 38 V, were applied to four IDTs placed in the x and y-directions (all were excited in the E-E mode). Subsequently, the temporal phase shift of the IDTs in the x-direction, θ_x, was fixed at 280°, while only θ_y of the IDTs in the y-direction was changed to adjust the velocity and the direction of the droplet actuated along the y-direction. Specifically, when θ_y was equal to 280°, the droplet moved along an oblique line of 45° on the substrate, and the trajectory is shown in Fig. 10(b). When θ_y equaled 220°, the droplet can be actuated to be transported along an oblique line at 30°, with the trajectory shown in Fig. 10(c). Similarly, when θ_y was set to 80° and 140°, the droplets can move along the oblique lines at -45° and -25° respectively, as shown in Fig. 10(d) and (e).

In addition, the droplet can be also transported along more complex routes. The SAW device developed in this work was excited in the E-E mode, by sequentially adjusting θ_x and θ_y within the ranges of (0, 180°) and (180°, 360°), respectively. Fig. 11 shows the time-lapsed 'H, I, T - shaped' trajectories of the droplet. Herein, an Arduino Due board was used as the main controller in the SAW generator developed by the authors, to control a Direct Digital Synthesis technology-based chip (DDS chip) to output high-frequency signals (Channel 1-4) with independently adjustable frequencies, amplitudes and phase shifts, which were applied to the four IDTs to excite the SAW, after being amplified by power amplifiers. The change of the values of the phase shift of Channel 1 and Channel 2 (that is, θ_x) and that of Channel 3 and Channel 4 (that is, θ_y) was pre-programmed in the Arduino to control the movement of the droplet along the trajectories designed. Taking the 'H - shaped' trajectory as an example, the sequence of the adjustment of the phase shifts was as follows (i) θ_x =0° and θ_y =80° for 3s, (ii) θ_x =0° and θ_y =280° for 1.5s, (iii) θ_x =280° and θ_y =0° for 2s, (iv) θ_x =0° and θ_y =280° for 1.5s, (v) θ_x =0° and θ_y =80° for 3s.
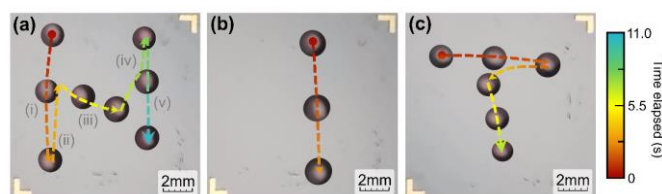
Fig. 11 (see Video S5~S7) Time-lapsed 'H, I, T - shaped' droplet trajectories using the E-E mode, respectively shown in (a), (b), and (c).   Here U_0=38 V, f=20.40 MHz, (Scale bars: 2 mm).   Here in each illustration of the control of the droplet transportation, the IDTs were excited in the E-E mode, and the droplet was placed on the substrate and was kept still for 5 seconds, where the initial phase shifts were set to be θ_x =0, θ_y=0.   Then the phase shifts began to be changed, and thus the droplet began to move.   The colours of the trajectories in the graphs represent the time scale from the beginning of the droplet movement.   The temperature of the droplet before and after the movement was measured to be (a) 33.4℃ - 39.9℃, (b) 33.2℃ - 37.5℃, (c) 32.7℃ - 38.8℃ (where the experiments were carried out at room temperature of ~25 ℃).

Conclusions

In this paper, the method of actuating droplets by exciting mixed TSAW and SSAW on the surface of a piezoelectric substrate, using the Exciter-Exciter mode, has been proposed.   Firstly, the vibrational equation of the mixed waves formed on the substrate in the E-E mode has been described, and the expression for the amplitude and the direction of the TSAW component of the mixed waves has been derived.   On this basis, a method for the adjustment of the velocity and direction of the droplets through changing the temporal phase shift, θ, actuated by the SAW device used and excited in the E-E mode, has been proposed theoretically.

Following that, a one-dimensional SAW device was fabricated and used to actuate the droplets loaded on the substrate, where two advantages of the E-E mode, compared with the routine E-A mode, have been demonstrated.   These are (1) the velocity and the direction of the actuated droplets can be adjusted by changing only θ, which can improve the convenience and programmability of making this adjustment, and (2) the velocity of the actuated droplets can be significantly increased.   Moreover, on-chip droplet transportation along different trajectories has been carried out, by adjusting the value of θ of the IDTs on a two-dimensional SAW device.   Here this use of the E-E mode provides an alternative method to actuate the droplets, which is important for several 'lab-on-a-chip' applications, used in the fields of chemical analysis and biomedical research.

Author Contributions

Mingyang Sui: Writing - original draft, Methodology, Formal Analysis. **Huijuan Dong**: Writing - review & editing, Methodology. **Guanyu Mu**: Data curation. **Jingze Xia**: Visualization. **Jie Zhao**: Methodology, Conceptualization. **Zhen Yang**: Methodology, Formal Analysis. **Tianlong Li**: Visualization. **Tong Sun**: Investigation. **K.T.V. Grattan**: Conceptualization, Writing - review & editing.

Conflicts of interest

There are no conflicts to declare.

Acknowledgements

Notes and references

1. L. Shang, Y. Cheng and Y. Zhao, *Chem Rev*, 2017, **117**, 7964-8040.
2. D. Wlodkowic and J. M. Cooper, *Curr Opin Chem Biol*, 2010, **14**, 556-567.
3. G. Schneider, *Nat Rev Drug Discov*, 2018, **17**, 97-113.
4. Y. Chen, A. J. Chung, T. H. Wu, M. A. Teitell, D. Di Carlo and P. Y. Chiou, *Small*, 2014, **10**, 1746-1751.
5. P. Li, Z. Mao, Z. Peng, L. Zhou, Y. Chen, P. H. Huang, C. I. Truica, J. J. Drabick, W. S. El-Deiry, M. Dao, S. Suresh and T. J. Huang, *Proc Natl Acad Sci U S A*, 2015, **112**, 4970-4975.
6. S. Zhao, D. Sun, J. Zhang, H. Lu, Y. Wang, R. Xiong and K. T. V. Grattan, *Materials Today Nano*, 2022, **18**.
7. K. Choi, A. H. Ng, R. Fobel and A. R. Wheeler, *Annu Rev Anal Chem (Palo Alto Calif)*, 2012, **5**, 413-440.
8. M. A. Qasaimeh, T. Gervais and D. Juncker, *Nat Commun*, 2011, **2**, 464.
9. J. Xie, F. Li, S. Kuang, H. Yang, X. Li, S. Tang, W. Li and S. Zhang, *IEEE/ASME Transactions on Mechatronics*, 2020, **25**, 942-950.
10. R. Xue, W. Liu, T. Jiang, C. Song, H. Jiang and Y. Ren, *Advanced Materials Interfaces*, 2020, **7**.
11. X. Fan, M. Sun, L. Sun and H. Xie, *Advanced Functional Materials*, 2020, **30**.

12. J. Li, T. Li, T. Xu, M. Kiristi, W. Liu, Z. Wu and J. Wang, *Nano Lett*, 2015, **15**, 4814-4821.
13. P. Zhang, H. Bachman, A. Ozcelik and T. J. Huang, *Annu Rev Anal Chem (Palo Alto Calif)*, 2020, **13**, 17-43.
14. A. R. Rezk, O. Manor, J. R. Friend and L. Y. Yeo, *Nat Commun*, 2012, **3**, 1167.
15. J. H. Jung, G. Destgeer, B. Ha, J. Park and H. J. Sung, *Lab Chip*, 2016, **16**, 3235-3243.
16. L. Li, N. Gu, H. Dong, B. Li and K. T. V. G, *RSC Advances*, 2020, **10**, 44593-44600.
17. Y. Ai, C. K. Sanders and B. L. Marrone, *Anal Chem*, 2013, **85**, 9126-9134.
18. D. J. Collins, B. Morahan, J. Garcia-Bustos, C. Doerig, M. Plebanski and A. Neild, *Nature Communications*, 2015, **6**.
19. Y. Gu, C. Chen, Z. Mao, H. Bachman, R. Becker, J. Rufo, Z. Wang, P. Zhang, J. Mai, S. Yang, J. Zhang, S. Zhao, Y. Ouyang, D. T. W. Wong, Y. Sadovsky and T. J. Huang, *Sci Adv*, 2021, **7**.
20. D. Foresti, M. Nabavi, M. Klingauf, A. Ferrari and D. Poulikakos, *Proc Natl Acad Sci U S A*, 2013, **110**, 12549-12554.
21. S. P. Zhang, J. Lata, C. Chen, J. Mai, F. Guo, Z. Tian, L. Ren, Z. Mao, P. H. Huang, P. Li, S. Yang and T. J. Huang, *Nat Commun*, 2018, **9**, 2928.
22. R. Tao, G. McHale, J. Reboud, J. M. Cooper, H. Torun, J. Luo, J. Luo, X. Yang, J. Zhou, P. Canyelles-Pericas, Q. Wu and Y. Fu, *Nano Lett*, 2020, **20**, 3263-3270.
23. A. Marzo, S. A. Seah, B. W. Drinkwater, D. R. Sahoo, B. Long and S. Subramanian, *Nat Commun*, 2015, **6**, 8661.
24. T. Vasileiou, D. Foresti, A. Bayram, D. Poulikakos and A. Ferrari, *Sci Rep*, 2016, **6**, 20023.
25. Z. Zhong, H. Zhu, P. Zhang, J. Morizio, T. J. Huang and K. Chakrabarty, *IEEE Trans Biomed Circuits Syst*, 2020, **14**, 1065-1078.
26. P. Zhang, C. Chen, F. Guo, J. Philippe, Y. Gu, Z. Tian, H. Bachman, L. Ren, S. Yang, Z. Zhong, P. H. Huang, N. Katsanis, K. Chakrabarty and T. J. Huang, *Lab Chip*, 2019, **19**, 3397-3404.
27. P. Zhang, C. Chen, X. Su, J. Mai, Y. Gu, Z. Tian, H. Zhu, Z. Zhong, H. Fu, S. Yang, K. Chakrabarty and T. J. Huang, *Sci Adv*, 2020, **6**, eaba0606.
28. R. Tao, J. Reboud, H. Torun, G. McHale, L. E. Dodd, Q. Wu, K. Tao, X. Yang, J. T. Luo, S. Todryk and Y. Fu, *Lab Chip*, 2020, **20**, 1002-1011.
29. T. Fukaya and J. Kondoh, *Japanese Journal of Applied Physics*, 2015, **54**.
30. X. Qin, X. Wei, L. Li, H. Wang, Z. Jiang and D. Sun, *Lab Chip*, 2021, **21**, 3165-3173.
31. Z. J. Jiao, X. Y. Huang and N. T. Nguyen, *Journal of Physics A: Mathematical and Theoretical*, 2008, **41**.
32. M. K. Tan, J. R. Friend and L. Y. Yeo, *Phys Rev Lett*, 2009, **103**, 024501.
33. S. B. Burnside, K. Pasieczynski, A. Zarareh, M. Mehmood, Y. Q. Fu and B. Chen, *Phys Rev E*, 2021, **104**, 045301.
34. P. Brunet and M. Baudoin, *Experiments in Fluids*, 2022, **63**.
35. Z. Guttenberg, H. Muller, H. Habermuller, A. Geisbauer, J. Pipper, J. Felbel, M. Kielpinski, J. Scriba and A. Wixforth, *Lab Chip*, 2005, **5**, 308-317.
36. Z. Ma, D. J. Collins and Y. Ai, *Anal Chem*, 2016, **88**, 5316-5323.
37. D. Sun, K. F. Bohringer, M. Sorensen, E. Nilsson, J. S. Edgar and D. R. Goodlett, *Lab Chip*, 2020, **20**, 3269-3277.
38. Y. Wu, R. Chattaraj, Y. Ren, H. Jiang and D. Lee, *Anal Chem*, 2021, **93**, 7635-7646.
39. J. Bennes, S. Alzuaga, F. Cherioux, S. Ballandras, P. Vairac, J. F. Manceau and F. Bastien, *IEEE Trans Ultrason Ferroelectr Freq Control*, 2007, **54**, 2146-2151.
40. A. Wixforth, C. Strobl, C. Gauer, A. Toegl, J. Scriba and Z. v Guttenberg, *Anal Bioanal Chem*, 2004, **379**, 982-991.
41. M. K. Tan, J. R. Friend and L. Y. Yeo, *Lab Chip*, 2007, **7**, 618-625.
42. V. Bussiere, A. Vigne, A. Link, J. McGrath, A. Srivastav, J. C. Baret and T. Franke, *Anal Chem*, 2019, **91**, 13978-13985.
43. J. Reboud, Y. Bourquin, R. Wilson, G. S. Pall, M. Jiwaji, A. R. Pitt, A. Graham, A. P. Waters and J. M. Cooper, *Proc Natl Acad Sci U S A*, 2012, **109**, 15162-15167.
44. A. Renaudin, P. Tabourier, V. Zhang, J. C. Camart and C. Druon, *Sensors and Actuators B: Chemical*, 2006, **113**, 389-397.
45. Y. Ai and B. L. Marrone, *Microfluidics and Nanofluidics*, 2012, **13**, 715-722.
46. N. Zhang, A. Horesh and J. Friend, *Adv Sci*, 2021, **8**, 2100408.
47. P. Brunet, M. Baudoin, O. B. Matar and F. Zoueshtiagh, *Phys Rev E Stat Nonlin Soft Matter Phys*, 2010, **81**, 036315.
48. S. M. Sheikholeslam Noori, M. Taeibi Rahni and S. A. Shams Taleghani, *Microgravity Science and Technology*, 2020, **32**, 647-660.
49. S. Yang, Z. Tian, Z. Wang, J. Rufo, P. Li, J. Mai, J. Xia, H. Bachman, P. H. Huang, M. Wu, C. Chen, L. P. Lee and T. J. Huang, *Nat Mater*, 2022, **21**, 540-546.
50. S. Li, X. Ding, F. Guo, Y. Chen, M. I. Lapsley, S. C. Lin, L. Wang, J. P. McCoy, C. E. Cameron and T. J. Huang, *Anal Chem*, 2013, **85**, 5468-5474.
51. P. Zhang, J. Rufo, C. Chen, J. Xia, Z. Tian, L. Zhang, N. Hao, Z. Zhong, Y. Gu, K. Chakrabarty and T. J. Huang, *Nat Commun*, 2021, **12**, 3844.
52. D. Koyama, T. Ide, J. R. Friend, K. Nakamura and S. Ueha, *IEEE Trans Ultrason Ferroelectr Freq Control*, 2007, **54**, 597-604.
53. J. Zhao, G. Mu, H. Dong, T. Sun and K. T. V. Grattan, *Mechanical Systems and Signal Processing*, 2022, **168**.
54. G. Mu, J. Zhao, H. Dong, J. Wu, K. T. V. Grattan and T. Sun, *Smart Materials and Structures*, 2021, **30**.
55. C. Devendran, N. R. Gunasekara, D. J. Collins and A. Neild, *RSC Advances*, 2016, **6**, 5856-5864.
56. A. I. ElSherbini and A. M. Jacobi, *J Colloid Interface Sci*, 2006, **299**, 841-849.
57. M. H. Biroun, M. Rahmati, M. Jangi, B. Chen and Y. Q. Fu, *International Journal of Multiphase Flow*, 2021, **136**.
58. M. S. Noori, M. T. Rahni and A. S. Taleghani, *Theoretical and Computational Fluid Dynamics*, 2020, **34**, 145-162.
59. M. Baudoin, P. Brunet, O. Bou Matar and E. Herth, *Applied Physics Letters*, 2012, **100**.